

Article

Platinum-Modified Rod-like Titania Mesocrystals with Enhanced Photocatalytic Activity

Zhishun Wei ^{1,2} , Yuanyuan Ji ¹ , Zuzanna Bielan ³ , Xin Yue ¹, Yuqi Xu ¹, Jiajie Sun ¹, Sha Chen ^{1,2,*}, Guoqiang Yi ^{1,2}, Ying Chang ^{1,2} and Ewa Kowalska ^{1,3,*} 

- ¹ Hubei Provincial Key Laboratory of Green Materials for Light Industry, New Materials and Green Manufacturing Talent Introduction and Innovation Demonstration Base, Hubei University of Technology, Wuhan 430068, China; wei.zhishun@hbut.edu.cn (Z.W.); 102100464@hbut.edu.cn (Y.J.); yuexin6912@163.com (X.Y.); 102300431@hbut.edu.cn (Y.X.); sjj73727@163.com (J.S.); yiguoqiang@hbut.edu.cn (G.Y.); cy0025@hbut.edu.cn (Y.C.)
- ² Hubei Longzhong Laboratory, Xiangyang 441000, China
- ³ Faculty of Chemistry, Jagiellonian University, 30-387 Krakow, Poland; zuzanna.bielan@uj.edu.pl
- * Correspondence: chensha@hbut.edu.cn (S.C.); ewa.k.kowalska@uj.edu.pl (E.K.)

Abstract: Photocatalysis is considered as an environmentally friendly method for both solar energy conversion and environmental purification of water, wastewater, air, and surfaces. Among various photocatalytic materials, titania is still the most widely investigated and applied, but more efforts must be carried out considering the synthesis of highly efficient photocatalysts for multifarious applications. It is thought that nanoengineering design of titania morphology might be the best solution. Accordingly, here, titania mesocrystals, assembled from crystallographically oriented nanocrystals, have been synthesized by an easy, cheap, and “green” solvothermal method (without the use of surfactants and templates), followed by simple annealing. The obtained materials have been characterized by various methods, including transmission electron microscopy (TEM), scanning electron microscopy (SEM), X-ray photoelectron spectroscopy (XPS), X-ray powder diffraction (XRD) and diffuse reflectance spectroscopy (DRS). It has been found that the as-obtained photocatalysts exhibit a unique nanorod-like subunit structure with excellent crystalline and surface properties. However, pristine titania is hardly active for a hydrogen evolution reaction, and thus additional modification has been performed by platinum photodeposition (and silver as a reference). Indeed, the modification with only 2 wt% of noble metals results in a significant enhancement in activity, i.e., ca. 75 and 550 times by silver- and platinum-modified samples, respectively, reaching the corresponding reaction rates of 37 $\mu\text{mol h}^{-1}$ and 276 $\mu\text{mol h}^{-1}$. Additionally, titania mesocrystals exhibit high oxidation power under simulated solar light irradiation for the degradation of antibiotics within the tetracycline group (tetracycline (TC), ciprofloxacin (CIP), norfloxacin (NOR) and oxytetracycline hydrochloride (OTC)). It has been found that both experimental results and the density functional theory (DFT) calculations confirm the high ability of titania mesocrystals for oxidative decomposition of tetracycline antibiotics.

Keywords: antibiotic degradation; titania; nanoengineering; mesocrystals; photocatalysis; Pt nanoparticles



Citation: Wei, Z.; Ji, Y.; Bielan, Z.; Yue, X.; Xu, Y.; Sun, J.; Chen, S.; Yi, G.; Chang, Y.; Kowalska, E. Platinum-Modified Rod-like Titania Mesocrystals with Enhanced Photocatalytic Activity. *Catalysts* **2024**, *14*, 283. <https://doi.org/10.3390/catal14040283>

Academic Editor: Roberto Fiorenza

Received: 19 March 2024

Revised: 10 April 2024

Accepted: 20 April 2024

Published: 22 April 2024



Copyright: © 2024 by the authors. Licensee MDPI, Basel, Switzerland. This article is an open access article distributed under the terms and conditions of the Creative Commons Attribution (CC BY) license (<https://creativecommons.org/licenses/by/4.0/>).

1. Introduction

Major current environmental problems include climate change, pollution, environmental degradation, and resource depletion. Accordingly, lots of research studies have been carried out to solve these issues, covering both the limitation of human/animal activity and environmental purification and recovery. Considering the latter, semiconductor-based photocatalysis is regarded as a promising technology to utilize solar energy for environmental purification and “green” generation of chemical fuels (e.g., via water splitting and carbon dioxide reduction) [1–3]. To date, remarkable progress on applied photocatalysis has been made, and various materials have already been developed [4–6]. Among them,

titania (titanium(IV) oxide, TiO_2) as a landmark semiconductor photocatalyst has been extensively studied, mainly due to its high efficiency, low price, stability (thermal, chemical and photochemical), and nontoxicity [7–10]. However, some problems connected with titania should also be mentioned:

- (i) Wide bandgap (ca. 3.20 eV), though profitable for good redox properties, also results in low light harvesting efficiency—only the UV range of the solar spectrum can be used;
- (ii) Recombination of charge carriers (typical for all semiconductors);
- (iii) Slow migration (transfer) of generated charge carriers (resulting from charge carriers' recombination, permanent trapping in deep electron traps, amorphous phase content, irregular structure, etc.).

Accordingly, various methods have been proposed to overcome all these problems, such as surface modification (with ions of metals and nonmetals, complexes, clusters and particles [11–15]), doping [16–18] (including self-doping [19–21]), and the formation of heterostructures with other materials (mainly via type-II heterojunction and Z-/S-scheme systems [22–25]). Indeed, modified titania photocatalysts exhibit both enhanced performance under UV irradiation and activity under visible light. However, the appearance of a vis response might also cause a decrease in UV activity since some modifiers (e.g., dopants) could work as a charge carriers' recombination center. Accordingly, the overall effect, i.e., the performance under both UV and vis irradiation, might not result in a real activity increase in all cases.

Fortunately, another method of titania performance enhancement has been proposed, i.e., nanoarchitecture design of titania photocatalysts. Indeed, it has been found that the preparation of titania with well-controlled/defined morphology is an effective method to overcome two (above mentioned) shortcomings (i.e., charge carriers' recombination (ii) and slow charges' migration (iii)). Probably, the faceted titania particles are the simplest examples of highly efficient structures with controlled morphology. For example, octahedral anatase particles (OAP) with eight {101} facets (bipyramid) exhibit exceptionally high photocatalytic performance, especially for reduction-based reactions and as a plasmonic photocatalyst (i.e., when modified with deposits of noble metals) because of the fast migration of photogenerated electrons via shallow electron traps [26–28]. Moreover, it has been found that the introduction of additional facet(s) might be beneficial for activity enhancement. Indeed, decahedral anatase particles (DAP) with eight {101} and two {001} facets exhibit the best photocatalytic performance among dozens of titania samples [29–33]. It has already been proven that spatial charge separation, i.e., electrons' and holes' migration towards {101} and {001} facets, respectively, is the main reason behind the exceptionally good photocatalytic performance of DAP [34]. However, it should be pointed out that not only the faster charge carriers' migration, but also other factors, e.g., the ability for water adsorption (resulting in more efficient formation of reactive oxygen species), must be considered for the overall performance [31,35–38]. For example, a recent study on mesoporous microballs built of faceted anatase particles has shown that DAP-based samples exhibit higher photocatalytic activity than OAP ones, despite worse charge carriers' separation, due to their higher hydrophilicity [39].

Next, more advanced titania structures have also been proposed, such as nanotubes [40,41], inverse opals [42,43] and mesocrystals [44–46], which have exhibited improved photocatalytic properties. However, most proposed synthesis methods (especially on the preparation of mesocrystals) are based on the addition of organic compounds during synthesis, which might cause both environmental issues and the possible impurity of the final product [34,45,47–49]. Moreover, even with such advanced morphology formation, TiO_2 -based photocatalytic materials could respond only to ultraviolet light (as already pointed above). Accordingly, it is thought that surface modification with noble metals, especially platinum, might cause the preparation of samples with the best performance under both UV and vis ranges of irradiation (and is thus preferable for natural environmental conditions, i.e., under direct sunlight). This is caused by the double action of noble metals, i.e., as an

electron sink, hindering the charge carriers' recombination under UV (known for more than forty years since the study by Allen J. Bard [50–53]), and as a “plasmonic sensitizer” under vis (due to plasmon resonance feature via energy or/and “hot” electron transfer), resulting in the appearance of a vis response [54–59].

Therefore, this work has proposed a simple solvothermal method, followed by annealing, for the synthesis of rod-like titania mesocrystals without using any additional template and morphology-regulating materials. For the further improvement of photocatalytic performance in both oxidation and reduction reactions, the effect of platinum (and silver as a reference) deposition on the surface of titania mesocrystals has been investigated. Additionally, the DFT calculations have been performed in order to understand the possible mechanism of antibiotics' degradation.

2. Results and Discussion

2.1. Structural Characterization of Unmodified Rod-like Titania Mesocrystals

The successful preparation of titania mesocrystals (the white powder after solvothermal reaction) has been confirmed by various methods. Firstly, the crystalline properties of unmodified samples have been investigated, and the obtained data are shown in Figure 1. Indeed, PTR sample (before annealing) shows almost no peaks in the XRD pattern, confirming its practically amorphous characteristics. In contrast, the XRD pattern of the annealed sample (TR) possesses highly intensive peaks, matching the standard anatase JCPDS card well (JCPDS-21-1272) [59]. Accordingly, it has been found that the TR sample is composed of pure anatase phase of titania with high crystallinity. Moreover, based on the Scherrer equation, i.e., $D = (K\lambda)/(\beta\cos\theta)$, where D , K , λ , β and θ are the mean size of the crystalline domains, a dimensionless shape factor, the X-ray wavelength, the line broadening at the full width at half maximum (FWHM) of analyzed peak (here 101) and the Bragg angle, respectively, the crystallite size of anatase, equal to 32 nm, has been estimated.

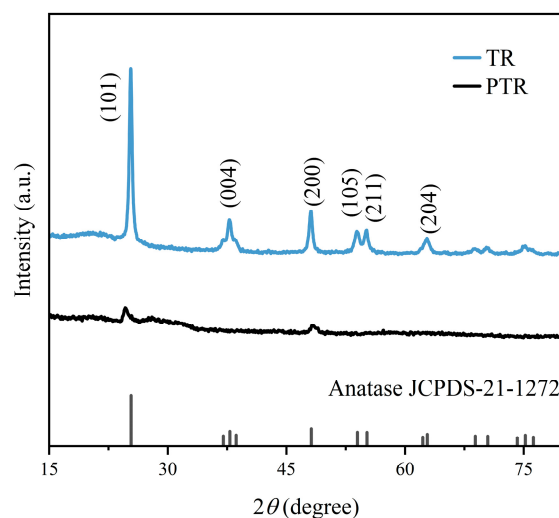


Figure 1. XRD patterns of PTR and TR samples.

Next, the morphology of samples has been examined, and the representative SEM and TEM images of PTR and TR samples are shown in Figures 2 and 3, respectively. In the case of amorphous sample (Figure 2), it is clear that it is in the form of porous rods (similar to rhubarb stalks), with an average length of about 1 μm . An enlarged image, shown in Figure 2b, reveals that each structure consists of diminutive nanorod-like subunits.

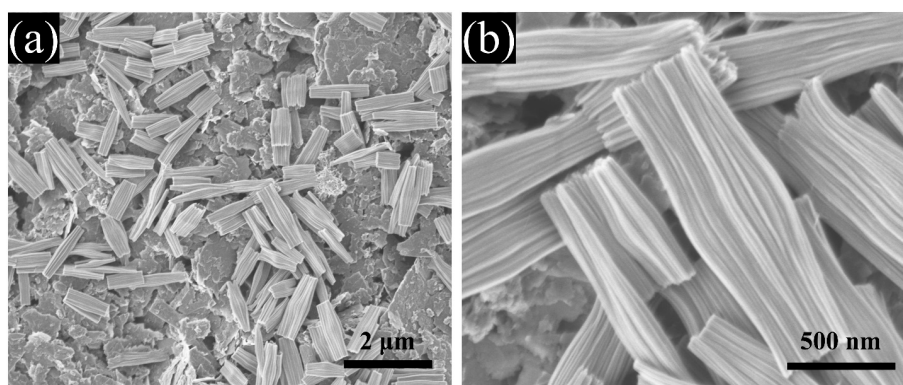


Figure 2. SEM images of PTR sample: (a) low magnification; (b) high magnification.

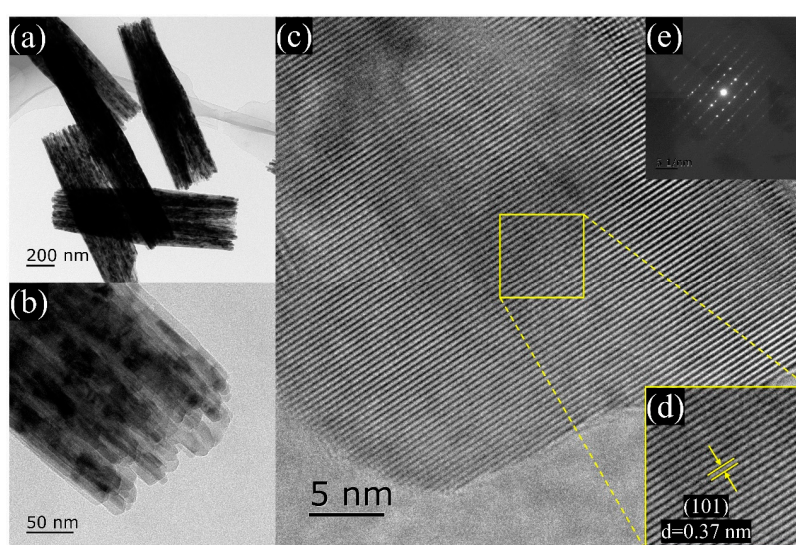


Figure 3. TEM observations of TR sample: (a) low magnification of TEM; (b) high magnification of TEM; (c) high resolution TEM (HR-TEM); (d) magnification of HR-TEM; and (e) SAED image.

The detailed analysis of titania sample after annealing (TR sample) has been performed by transmission electron microscopy (TEM), and the results are shown in Figure 3a–e. Similarly to the PTR sample, the TR one exhibits a rod-like morphology, composed of fine nanorod-like subunits, with visible gaps between them (Figure 3a,b). However, high-resolution TEM (HRTEM) images (Figure 3c,d) reveal the crystal nature of this sample with the lattice spacing of the nanorod-like subunits of about 0.37 nm, indicating that the rods have grown in the direction of (101) [60]. Additionally, the selective area electron diffraction (SAED) analysis, presented in Figure 3e, shows the [101] zone axis of anatase phase, indicating a single-crystal-like structure with highly ordered directional distribution. Moreover, the slightly elongated diffraction spots indicate a certain lattice mismatch between the boundaries, which corresponds well to the structural characteristics of mesocrystals [61].

2.2. Characterization of the Pt-Modified Rod-like Titania Mesocrystals

For the activity improvements, the rod-like titania mesocrystals (TR sample) have been modified with platinum nanoparticles (NPs). Obviously, the basic morphology of the TR sample has not been changed, and the Pt/TR photocatalyst keeps a rod-like shape, composed of titania mesocrystals, as shown in Figure 4a. There is only one difference between the Pt/TR and TR samples, i.e., the presence of platinum deposits, uniformly distributed on the whole sample surface in the case of the latter. It has been found that Pt NPs contain the lattice stripes of (111) orientation with lattice spacing of about 0.25 nm

(Figure 4b,c), which indicates that the mesocrystals' morphology is decisive for the formation of facet-oriented Pt NPs, as similarly reported by Kelly et al. for lattice parameter evolution in Pt NPs (during sintering and grain growth) [62].

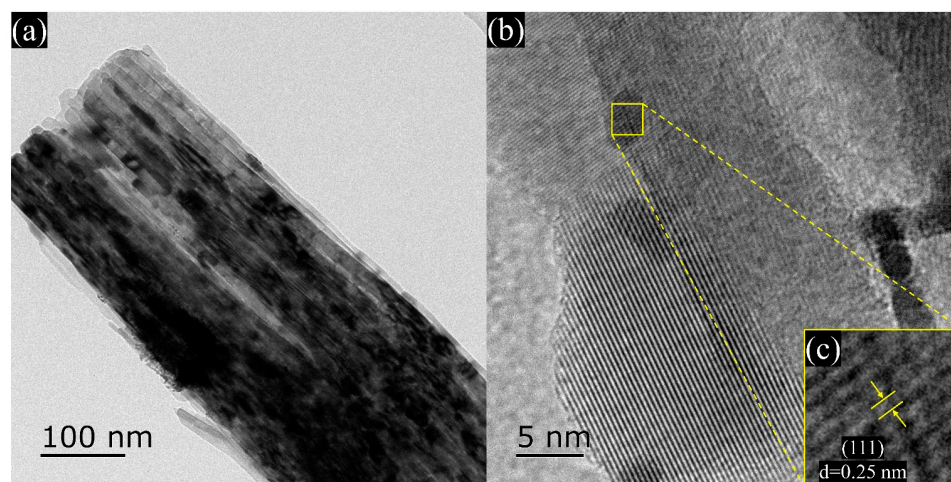


Figure 4. TEM observations of Pt/TR sample: (a) TEM; (b) HR-TEM; and magnification of HR-TEM; (c) magnification of HR-TEM.

Next, the surface properties of Pt/RT sample have been evaluated by X-ray photoelectron spectroscopy (XPS). Interestingly, it has been found that +4 oxidation state is the only oxidation state of titanium in this sample, as clearly observed on deconvoluted Ti 2p peaks, showing two single peaks at ca. 458.9 eV and 464.6 eV for Ti 2p_{3/2} and Ti 2p_{1/2}, respectively (Figure 5a). This is in contrast to many other studies on titania (pristine and modified with noble metals), where usually at least a small percentage of a reduced form of titanium (Ti³⁺) coexists in the sample [26,59,63,64]. Accordingly, it might be proposed that the formation of perfectly crystallized structure, such as titania mesocrystals, results in the preparation of samples with almost no defects. Similarly, the deconvolution of oxygen peak (O 1s) has resulted in the presence of only two forms of oxygen, i.e., Ti-O (oxygen in the crystal lattice of titania) and hydroxyl groups with a binding energy of ca. 530.0 eV and 531.2 eV, respectively (Figure 5b). According to the literature, the oxygen peak usually consists of three to five oxygen species, including O-Ti bonds in titania and titanium(III) oxide, O-H bonds in hydroxyl groups, O-C and O=C bonds and adsorbed water (H₂O) [64–67]. This finding also confirms the high crystal/surface purity of the titania mesocrystals obtained in this study. The XPS analysis of carbon shows only two peaks at ca. 284.8 eV and 288.25 eV, corresponding to C-C and C-OH bonds, respectively [68] (Figure 5c). Titania samples usually contain three forms of carbon, such as C-C, C-OH and C=O, resulting mainly from the atmosphere during the samples' preparation [66–68]. In the case of platinum, three different oxidation states could be distinguished, i.e., (i) the main form of zero-valent state (Pt⁰) at 71.2 eV and 74.5 eV, (ii) +2 oxidation state (Pt²⁺) at 72.1 eV and 75.4 eV, and (iii) +4 oxidation state (Pt⁴⁺) at 73.2 and 76.5 eV (Figure 5d). This indicates that though platinum has been successfully reduced during photodeposition (as expected), either the reduction reaction has been incomplete (low probability considering highly reduced conditions), or some stabilized forms of oxidized platinum have been formed. For example, it has been reported that Pt-Ti-O bonds might be formed during platinum reduction [69]. Although, there is no peak at Ti 2p spectrum indicating Pt-Ti-O bonds (at ca. 457 eV [69]), the possibility of other oxidized forms of platinum (e.g., blocks for Pt(II) complexes [70] or Ptⁿ⁺/Pt⁰ clusters [71,72]), stabilized within either platinum NPs, titania (on the surface or encapsulated in it) or at the Pt/TiO₂ interface, could not be rejected.

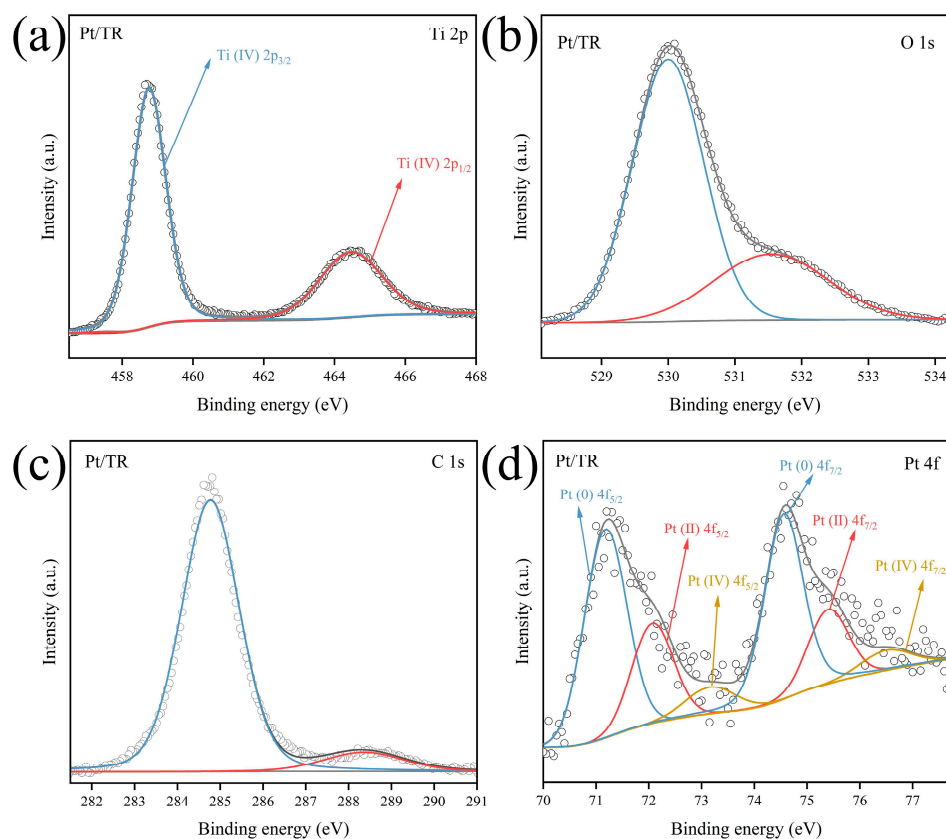


Figure 5. The deconvoluted XPS spectra for: (a) titanium (Ti 2p), (b) oxygen (O 1s), (c) carbon (C 1s) and (d) platinum (Pt 4f) of Pt/TR sample.

Next, the photoabsorption properties of pristine (TR) and noble metal-modified mesocrystals (platinum (Pt/TR) and silver (Ag/TR) as a reference) have been investigated, and the obtained data are shown in Figure 6. As expected, the photoabsorption of the TR sample (unmodified TiO₂ mesocrystals) is limited to the UV range (absorption edge at ca. 396 nm; Figure 6a), with a corresponding bandgap energy of ca. 3.13 eV, calculated from the Tauc plot (Figure 6b), which is a typical value for anatase titania (3.1–3.3 eV, depending on the crystal properties and defects' type/content [31,73–75]). After the surface modification with noble metals, the color of the samples changed from white to brown and grey for Ag/TR and Pt/TR, respectively. The photoabsorption at the visible-light range appears due to the localized surface plasmon resonance (LSPR) of these metals [76–79]. In the case of silver, a clear LSPR peak with a maximum at ca. 470 nm indicates the presence of spherical 20–50 nm sized Ag NPs [80–82]. In the case of platinum, usually, there is strong photoabsorption at the whole visible range (a typical grey color of platinum-modified samples) rather than a single LSPR peak (as shown in Figure 6a) [26,64,83–85]. Importantly, the presence of noble metals should not influence the bandgap energy since NPs are only deposited on the surface of titania. Indeed, as shown in Figure 6b, the bandgap energy is practically the same for all samples (a slight “apparent” shift might be observed towards larger energy since plasmon resonance of noble metals overlaps with photoabsorption by titania).

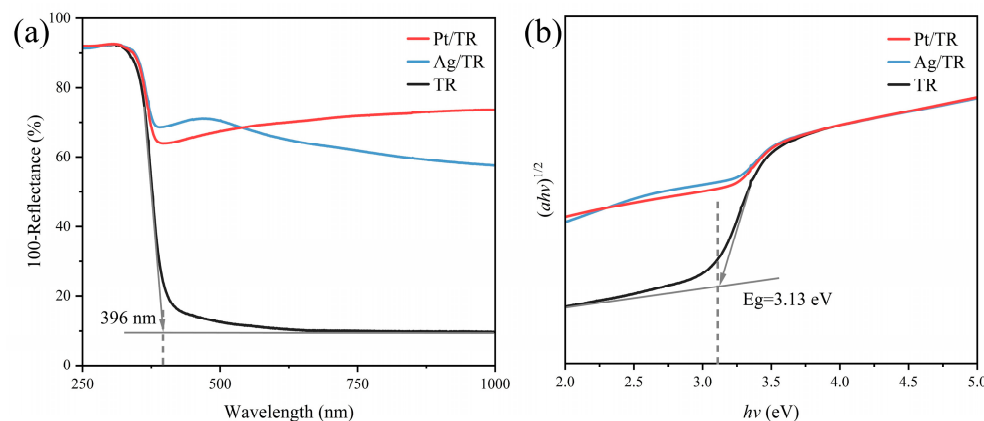


Figure 6. Photoabsorption properties of pristine and modified samples: (a) DRS spectra, and (b) Tauc plots.

2.3. Photocatalytic Performance Evaluation

The photocatalytic activity of pristine and modified titania mesocrystals has been investigated in both reduction and oxidation reactions. At first, the methanol dehydrogenation with H_2 generation was conducted, and the obtained data are shown in Figure 7. It should be pointed out that sole irradiation does not cause any effect, whereas the unmodified TR sample can hardly generate any hydrogen under full-light spectrum irradiation, with a H_2 evolution rate of only $0.5 \mu\text{mol}\cdot\text{h}^{-1}$. This is typical for pristine titania samples, being known for inactivity for hydrogen generation reaction due to high overvoltage of hydrogen evolution [26,64]. Accordingly, noble metals are commonly used as a cocatalyst for hydrogen formation. Indeed, the presence of silver and platinum results in a significant enhancement in activity by ca. 74 and 550 times, reaching reaction rates of $37 \mu\text{mol h}^{-1}$ and $276 \mu\text{mol h}^{-1}$, respectively. It should be pointed out that under UV irradiation, noble metals could play a double function when deposited on the surface of wide-bandgap semiconductors, i.e., (i) as a sink for electrons, hindering charge carriers' recombination (the formation of the Schottky barrier); and (ii) as a cocatalyst for some surface reactions (e.g., formation of hydrogen molecules). Much higher activity of Pt/TR than Ag/TR corresponds well to the higher work function of platinum than silver, and thus more efficient electron transfer from the conduction band of titania (and the larger Schottky barrier), as well as the smaller overvoltage for hydrogen generation [86–88].

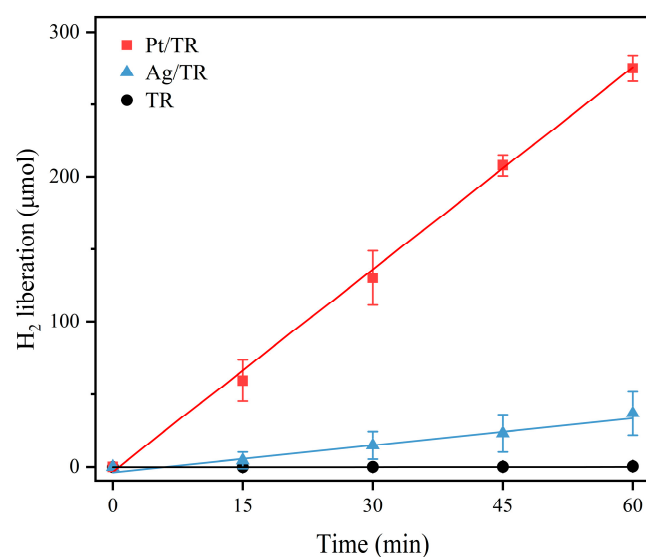


Figure 7. Photocatalytic activity for H_2 generation on rod-like titania mesocrystals: unmodified (TR) and modified with platinum (Pt/TR) and silver (Ag/TR).

Additionally, it should be pointed out that the linear evolution of hydrogen during irradiation confirms the high photo-stability of photocatalysts. Similar data have been achieved for other titania samples modified with noble metals, resulting from the well-known stability of titania as well as the stability of photo-deposited noble metals on its surface (the metal leaching is not expected under UV irradiation since noble metals work as an electron sink [26,64,89–92]).

In the next step, the photocatalytic performance of the obtained samples has been evaluated for oxidative degradation of tetracycline hydrochloride (TC) antibiotic under simulated solar light. First, simple photolysis (without photocatalyst) has been performed, and it has been confirmed that TC is not decomposed under sole irradiation. Then, adsorption–desorption equilibrium was achieved within 30 min stirring in the dark, with only ca. 5% of TC adsorption for all samples. As expected, the Pt/TR sample exhibits the best photocatalytic activity, with a TC degradation efficiency of 97.1% over 90 min of irradiation (Figure 8a), and a constant reaction rate of 0.044 min^{-1} (calculated according to pseudo-first-order kinetics formula), and thus showing ca. two times faster TC degradation than other samples (Figure 8b).

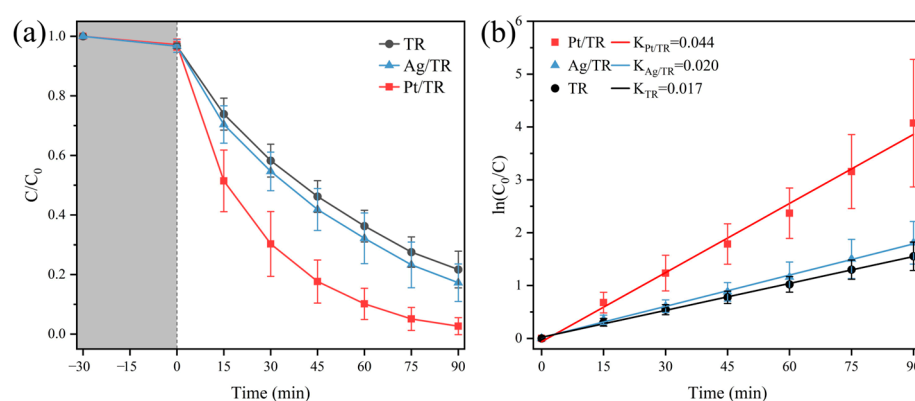


Figure 8. Photocatalytic activity of unmodified and modified titania mesocrystals: (a) efficiency of TC degradation; and (b) corresponding pseudo-first-order kinetics plots.

In order to further confirm the high activity of Pt/TR photocatalyst, other antibiotics from the tetracycline group, such as ciprofloxacin (CIP), norfloxacin (NOR) and oxytetracycline hydrochloride (OTC), have also been tested. Indeed, a very high decomposition rate of all tested antibiotics was achieved, as shown in Figure 9. Accordingly, it might be concluded that the Pt/TR sample has very high activity for both reduction and oxidation reactions.

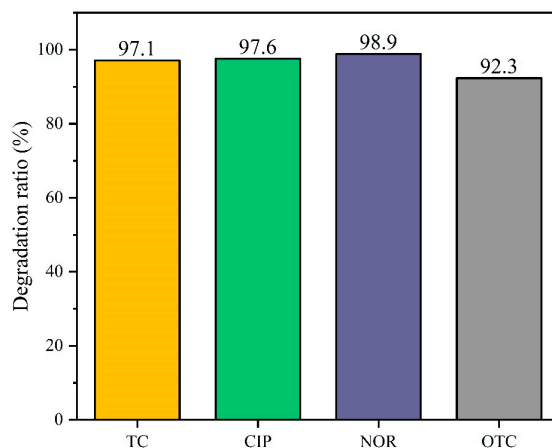


Figure 9. The results of photodegradation efficiency of Pt/TR against different antibiotics from tetracycline hydrochloride group.

In order to evaluate the (photo)stability of Pt/RT photocatalyst, recycling experiments were performed, i.e., TC degradation was repeated five times with neither changing of the photocatalyst nor of the reaction conditions. After each cycle, the photocatalyst was only washed with water, and then freeze-dried before the next cycle. It was found that the degradation efficiency decreased by ca. 20% after five cycles. It has been proposed that, probably, an inefficient amount of photocatalyst is responsible for the activity drop since it is impossible to recover all photocatalyst particles after each cycle. It should be pointed out that in the case of photocatalytic reactions, usually the optimal conditions (maximum photoabsorption) are reached for a much larger photocatalyst content (1–2 g/L [93]) than that used here (0.3 g/L, to limit the cost of the photocatalyst containing platinum). Therefore, the recycling experiments were additionally repeated for a much larger photocatalyst amount, i.e., 1.5 g/L, as shown in Figure 10b. Indeed, it has been found that TC degradation is both much more efficient (99%) and stable (same effect for five subsequent cycles) with an increase in the photocatalyst content.

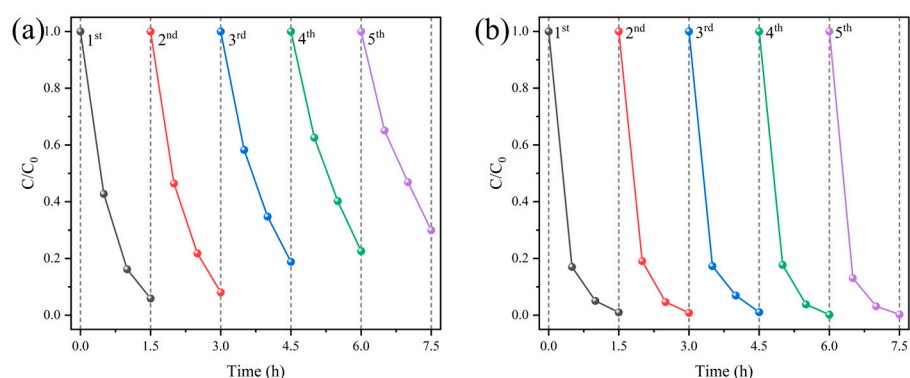


Figure 10. The recycling experiments for photocatalytic degradation of TC (100 mL) on Pt/TR for photocatalyst content of: (a) 30 mg; and (b) 150 mg.

The photocatalytic effect on antibiotics' photodegradation was further verified by density functional theory (DFT) calculation, based on the Fukui function, and the obtained results are shown in Figures 11 and S1–S3, and Tables S1–S4. Based on the optimized TC molecular structure (Figure 11a), the electrostatic potential (ESP) diagram, and occupied (HOMO) and unoccupied (LUMO) molecular orbitals regions have been designated. It is proposed that the blue parts, shown in Figure 11b, representing hydroxyl and carbonyl regions, are vulnerable to radical attack and destruction. Meanwhile, Figure 11c shows that the HOMO region of TC is mainly located in the phenolic hydroxyl group and benzene ring, while the LUMO region of TC (Figure 11d) is located near the dimethyl group. Accordingly, the benzene ring region in TC is relatively stable and difficult to be destroyed, whereas the dimethyl group in LUMO region might be easily damaged by nucleophilic free radicals ($\bullet\text{O}_2^-$ and $\bullet\text{OH}$, formed during photocatalytic reactions [94–96]) due to their relatively active properties [97]. Moreover, the electrophilicity (f^-) and nucleophilicity (f^+) values of each atom in the TC molecule have been estimated by calculating Hirshfeld charges and corresponding Fukui index values, as presented in Table S1. The high f^- and f^+ values of the dimethyl atoms additionally indicate their high vulnerability [98]. Similar results have also been achieved for other antibiotics (CIP, NOR and OTC molecules), presented in the Supplementary Materials (Figures S2 and S3 and Tables S2–S4), confirming their degradation ability by photocatalytic reactions.

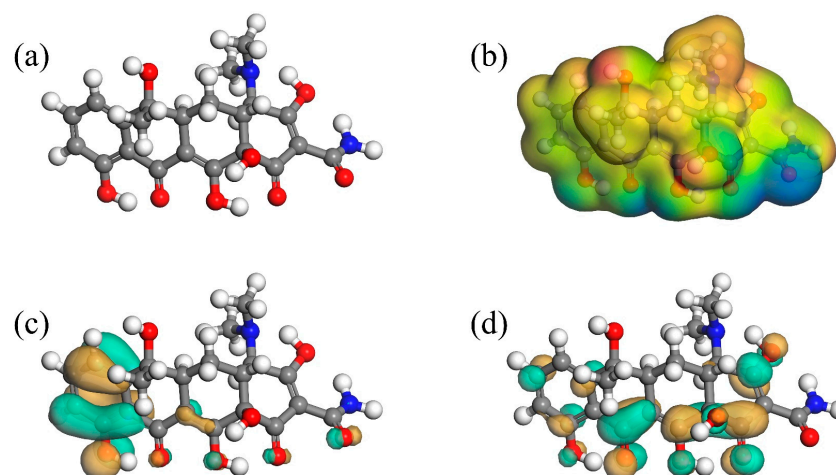


Figure 11. DFT calculation of: (a) optimized structure of TC; (b) ESP mapping of TC; (c) the HOMO, and (d) the LUMO regions in TC; gray—carbon, red—oxygen, blue—nitrogen, white—hydrogen.

3. Experimental Section

3.1. Materials

Anhydrous methanol (CH_3OH) and tetrabutyl titanate (TBOT) were purchased from Sinopharm Chemical Reagent Ltd. (Shanghai, China). Chloroplatinic acid hexahydrate ($\text{H}_2\text{PtCl}_6 \cdot 6\text{H}_2\text{O}$), silver nitrate (AgNO_3), tetracycline hydrochloride (TC), ciprofloxacin (CIP), norfloxacin (NOR) and oxytetracycline hydrochloride (OTC) were bought from Aladdin (Shanghai, China).

3.2. Synthesis of Rod-like Titania Mesocrystals

Rod-like titania mesocrystals were prepared by a simple solvothermal process, followed by annealing. Typically, TBOT (0.5 mL) and CH_3OH (59.5 mL) were placed in a 100-mL Teflon liner, and then ultrasonically dispersed for 10 min to ensure the uniformity of the reactants. After that, the Teflon liner was placed into an autoclave, and then thermally treated at $200\text{ }^\circ\text{C}$ for 24 h. After the reaction, the collected precipitate was washed twice with anhydrous methanol and twice with deionized water, centrifuged, and freeze-dried at $-85\text{ }^\circ\text{C}$ for 24 h. The obtained amorphous titania sample, marked as PTR, was annealed in a muffle furnace at $500\text{ }^\circ\text{C}$ for 2 h in order to obtain highly crystalline rod-like titania mesocrystals, marked as TR.

3.3. Synthesis of Pt-Modified Rod-like Titania Mesocrystals

The surface of titania mesocrystals was modified with NPs of platinum (or silver in the case of the reference sample) by the photodeposition method. This method is very convenient due to the fast and complete deposition of the whole metal content (complete reduction of metal cations [99]), and is thus often used for the surface modification of wide-bandgap semiconductors with noble metals [50,53,100–102]. It is based on the photo-generation of electrons, which are the main reductive species of respective metal cations. It should be pointed out that the formation of electrons in/on irradiated semiconductors facilitates the direct deposition of formed metal NPs on the semiconductor surface (ensuring the direct contact between semiconductor and noble metal). To avoid the recombination of electrons with holes, methanol (or another hole scavenger) is usually added before irradiation. Moreover, photodeposition is usually performed under anaerobic conditions to avoid electron scavenging by oxygen (though sometimes photodeposition is performed in the presence of oxygen/air, which might work as a morphology-control agent, e.g., to obtain finer and/or more uniform NPs [64,103]). Accordingly, the TR sample (200 mg) was dispersed with platinum precursor solution (2 wt% in respect to titania) in 25 mL of an ultrapure water–methanol solution (50 vol%), followed by Ar bubbling for oxygen removal. The sealed reaction tube was continuously illuminated for 1 h using a 400 W mercury lamp

(Bofeida Technology Co., LTD., Shenzhen, China). The obtained sample, marked as Pt/TR, was washed twice with methanol and twice with deionized water, centrifugally collected and freeze-dried for 24 h. In order to confirm the significant enhancement in photocatalytic activity by Pt nanoparticles, a reference sample with silver NPs was prepared analogously, and marked as Ag/TR.

3.4. Physicochemical and Photocatalytic Characterization of Obtained Samples

Crystallographic analysis (XRD) was performed on an X-ray diffractometer (XRD, Empyrean, Almelo, Netherlands). The morphology of the samples was determined using scanning electron microscopy (SEM, Hitachi SU8010, Tokyo, Japan) and transmission electron microscopy (TEM, JEOL JEM-F200, Tokyo, Japan). The light-absorption properties were measured using diffuse reflectance spectroscopy (DRS, Macy UV-1800, Shanghai, China). The bandgap energy of photocatalysts was calculated from the corresponding Kubelka–Munk function. The oxidation states of elements were determined by X-ray photoelectron spectroscopy (XPS, ULVAC-PHI5000 VesaProbe III, Chigasaki, Japan).

The photocatalytic activity was investigated in two reaction systems to check the performance in both reduction and oxidation reactions. Accordingly, the former was evaluated by hydrogen formation under ambient temperature (both the lamp and the irradiated sample tubes were cooled down by circulating water, as shown in Figures 12 and S4). In a typical experiment, 50 mg of photocatalyst was suspended in 5 mL of an ultrapure water solution containing methanol (50 vol%), followed by irradiation with a full spectrum of 400 W mercury lamp. The amount of generated hydrogen was measured every 15 min using gas chromatography (GC, FULI GC9790II, Wenling, China).

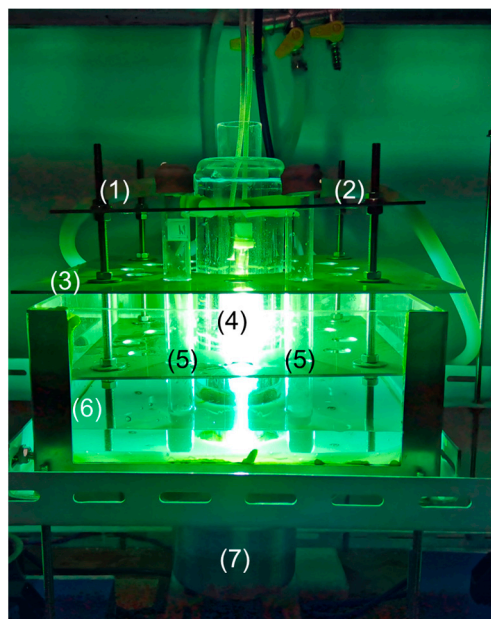


Figure 12. The photography of photoreactor system used for testing of hydrogen evolution reaction: (1) inlet of cooling water, (2) outlet of cooling water, (3) sample holder, (4) 400 W Hg lamp, (5) sample/tube reactors, (6) water bath, (7) magnetic stirrer.

The oxidation ability was tested for the degradation of the tetracycline (TC) antibiotic and other antibiotics from the tetracycline group (ciprofloxacin (CIP), norfloxacin (NOR) and oxytetracycline hydrochloride (OTC)) in a circulating cooling water system under simulated solar light, as shown in Figure S5. The photocatalyst (30 mg) was dispersed in 100 mL of the antibiotic solution (30 mg/L), and the suspension was stirred continuously in the dark for 30 min to achieve an adsorption–desorption equilibrium. Subsequently, the suspension was irradiated with a full spectrum illumination of a 300 W Xe lamp

(CEAULIGHT, Beijing, China), i.e., $\lambda = 200\sim 2500$ nm, and the distance between the light source and the reaction suspension of 10 cm. At regular time intervals, 3 mL of the suspension was collected, centrifuged (to separate the photocatalyst), and analyzed with UV-vis spectrophotometer (Macy UV-1800, Shanghai, China).

4. Conclusions

The rod-like titania mesocrystals could be easily prepared by a cheap, and simple solvothermal method without the use of any morphology-control agents, and thus via a “green” process. Although the properties and thus resulting activity of mesocrystals are very good, they could not be used for methanol dehydrogenation since pristine titania is inactive for a hydrogen evolution reaction (as well as simple photolysis without a photocatalyst). However, the modification of mesocrystals’ surface with only 2 wt% of noble metals causes a significant enhancement in activity (by as much as 550 times in the case of platinum). Additionally, both pristine and modified titania rods exhibit high activity for oxidative degradation of antibiotics from the tetracycline group, reaching even almost complete (ca. 99%) and stable degradation (over five subsequent cycles) for a photocatalyst content of 1.5 g/L. Both experimental data and theoretical calculations reveal the excellent performance of platinum-modified titania mesocrystals for the decomposition of antibiotics under solar-simulated light.

Accordingly, titania mesocrystals prepared by a “green” method and additionally modified with a low content of noble metals (especially with platinum) are excellent materials for solar-based environmental purification and fuel generation.

Supplementary Materials: The following supporting information can be downloaded at: <https://www.mdpi.com/article/10.3390/catal14040283/s1>, Figure S1: DFT calculations of: (a) optimized structure of CIP; (b) ESP mapping of CIP; (c) the HOMO; and (d) the LUMO distributions in CIP; Figure S2: DFT calculations of: (a) optimized structure of NOR; (b) ESP mapping of NOR; (c) the HOMO; and (d) the LUMO distributions in NOR; Figure S3: DFT calculations of: (a) optimized structure of OTC; (b) ESP mapping of OTC; (c) the HOMO; and (d) the LUMO distributions in OTC; Table S1: Hirshfeld charge and Fukui index values calculated for TC; Table S2: Hirshfeld charge and Fukui index values calculated for CIP; Table S3: Hirshfeld charge and Fukui index values calculated for NOR; Table S4: Hirshfeld charge and Fukui index values calculated for OTC; Figure S4: Schematic drawing of photoreactor system used for testing of H₂ evolution reaction; Figure S5: Schematic drawing of photoreactor system used for testing of TC degradation.

Author Contributions: Conceptualization, Z.W.; methodology, Z.W.; validation, Y.J. and Z.B.; data curation, Y.J. and Y.X.; investigation, Y.J., Y.X., X.Y., J.S., S.C., G.Y. and Y.C.; resources, Z.W.; writing—original draft preparation, Z.W., Y.J., Y.X., X.Y., J.S., S.C., G.Y., Y.C. and E.K.; writing—review and editing, Z.W., Z.B. and E.K.; supervision, Z.W. and E.K.; funding acquisition, Z.W. and E.K. All authors have read and agreed to the published version of the manuscript.

Funding: This research was funded by the National Natural Science Foundation of China (NSFC) (51802087), and the Green Industry Leading Program of Hubei University of Technology (XJ2021002101). This project is co-financed by the Polish National Agency for Academic Exchange within the Polish Returns Program (BPN/PPO/2021/1/00037) and the National Science Centre (2022/01/1/ST4/00026).

Data Availability Statement: The raw/processed data required to reproduce these findings cannot be shared at this time as the data also form part of an ongoing study.

Conflicts of Interest: The authors declare no conflicts of interest.

References

1. Hoffmann, M.R.; Martin, S.T.; Choi, W.Y.; Bahnemann, D.W. Environmental applications of semiconductor photocatalysis. *Chem. Rev.* **1995**, *95*, 69–96. [[CrossRef](#)]
2. Chen, S.S.; Qi, Y.; Hisatomi, T.; Ding, Q.; Asai, T.; Li, Z.; Ma, S.S.K.; Zhang, F.X.; Domen, K.; Li, C. Efficient Visible-Light-Driven Z-Scheme Overall Water Splitting Using a MgTa₂O_{6-x}N_y/TaON Heterostructure Photocatalyst for H₂ Evolution. *Angew. Chem. Int. Edit* **2015**, *54*, 8498–8501. [[CrossRef](#)]

3. Ogawa, K.; Suzuki, H.; Zhong, C.; Sakamoto, R.; Tomita, O.; Saeki, A.; Kageyama, H.; Abe, R. Layered Perovskite Oxyiodide with Narrow Band Gap and Long Lifetime Carriers for Water Splitting Photocatalysis. *J. Am. Chem. Soc.* **2021**, *143*, 8446–8453. [[CrossRef](#)] [[PubMed](#)]
4. Suzuki, H.; Higashi, M.; Tomita, O.; Ishii, Y.; Yamamoto, T.; Kato, D.; Kotani, T.; Ozaki, D.; Nozawa, S.; Nakashima, K.; et al. $\text{PbBi}_3\text{O}_4\text{X}_3$ (X = Cl, Br) with Single/Double Halogen Layers as a Photocatalyst for Visible-Light-Driven Water Splitting: Impact of a Halogen Layer on the Band Structure and Stability. *Chem. Mat.* **2021**, *33*, 9580–9587. [[CrossRef](#)]
5. Kim, E.S.; Nishimura, N.; Magesh, G.; Kim, J.Y.; Jang, J.W.; Jun, H.; Kubota, J.; Domen, K.; Lee, J.S. Fabrication of $\text{CaFe}_2\text{O}_4/\text{TaON}$ Heterojunction Photoanode for Photoelectrochemical Water Oxidation. *J. Am. Chem. Soc.* **2013**, *135*, 5375–5383. [[CrossRef](#)]
6. Verma, P.; Yuan, K.; Kuwahara, Y.; Mori, K.; Yamashita, H. Enhancement of plasmonic activity by Pt/Ag bimetallic nanocatalyst supported on mesoporous silica in the hydrogen production from hydrogen storage material. *Appl. Catal. B-Environ.* **2018**, *223*, 10–15. [[CrossRef](#)]
7. Kusiak-Nejman, E.; Morawski, A.W. TiO_2 /graphene-based nanocomposites for water treatment: A brief overview of charge carrier transfer, antimicrobial and photocatalytic performance. *Appl. Catal. B-Environ.* **2019**, *253*, 179–186. [[CrossRef](#)]
8. Markowska-Szczupak, A.; Endo-Kimura, M.; Paszkiewicz, O.; Kowalska, E. Are titania photocatalysts and titanium implants safe? Review on the toxicity of titanium compounds. *Nanomaterials* **2020**, *10*, 2065. [[CrossRef](#)] [[PubMed](#)]
9. Pichat, P. Fundamentals of TiO_2 Photocatalysis. Consequences for Some Environmental Applications. In *Heterogeneous Photocatalysis: From Fundamentals to Green Applications*; Colmenares, J.C., Xu, Y.-J., Eds.; Springer: Berlin/Heidelberg, Germany, 2016; pp. 321–359.
10. Gottuso, A.; De Pasquale, C.; Livraghi, S.; Palmisano, L.; Diré, S.; Ceccato, R.; Parrino, F. Nitrate radicals generated by TiO_2 heterogeneous photocatalysis: Application to the cleavage of C=C double bond to carbonyl compounds. *Mol. Catal.* **2023**, *550*, 113607. [[CrossRef](#)]
11. Mitoraj, D.; Kisch, H. The nature of nitrogen-modified titanium dioxide photocatalysts active in visible light. *Angew. Chem. Int. Ed.* **2008**, *47*, 9975–9978. [[CrossRef](#)]
12. Zabek, P.; Kisch, H. Polyol-derived carbon-modified titania for visible light photocatalysis. *J. Coord. Chem.* **2010**, *63*, 2715–2726. [[CrossRef](#)]
13. Kisch, H.; Sakthivel, S.; Janczarek, M.; Mitoraj, D. A low-band gap, nitrogen-modified titania visible-light photocatalyst. *J. Phys. Chem. C* **2007**, *111*, 11445–11449. [[CrossRef](#)]
14. Macyk, W.; Burgeth, G.; Kisch, H. Photoelectrochemical properties of platinum(IV) chloride surface modified TiO_2 . *Photochem. Photobiol. Sci.* **2003**, *2*, 322–328. [[CrossRef](#)] [[PubMed](#)]
15. Trochowski, M.; Kobielski, M.; Pucelik, B.; Dąbrowski, J.M.; Macyk, W. Dihydroxyanthraquinones as stable and cost-effective TiO_2 photosensitizers for environmental and biomedical applications. *J. Photochem. Photobiol. A Chem.* **2023**, *438*, 114517. [[CrossRef](#)]
16. Asahi, R.; Morikawa, T.; Ohwaki, T.; Aoki, K.; Taga, Y. Visible-light photocatalysis in nitrogen-doped titanium oxides. *Science* **2001**, *293*, 269–271. [[CrossRef](#)] [[PubMed](#)]
17. Ohno, T. Preparation of visible light active S-doped TiO_2 photocatalysts and their photocatalytic activities. *Wat. Sci. Technol.* **2004**, *49*, 159–163. [[CrossRef](#)]
18. Ohno, T.; Miyamoto, Z.; Nishijima, K.; Kanemitsu, H.; Xueyuan, F. Sensitization of photocatalytic activity of S- or N-doped TiO_2 particles by adsorbing Fe^{3+} cations. *Appl. Catal. A Gen.* **2006**, *302*, 62–68. [[CrossRef](#)]
19. Naldoni, A.; Allietta, M.; Santangelo, S.; Marelli, M.; Fabbri, F.; Cappelli, S.; Bianchi, C.L.; Psaro, R.; Dal Santo, V. Effect of Nature and Location of Defects on Bandgap Narrowing in Black TiO_2 Nanoparticles. *J. Am. Chem. Soc.* **2012**, *134*, 7600–7603. [[CrossRef](#)] [[PubMed](#)]
20. Han, X.X.; Huang, J.; Jing, X.X.; Yang, D.Y.; Lin, H.; Wang, Z.G.; Li, P.; Chen, Y. Oxygen-deficient black titania for synergistic/enhanced sonodynamic and photoinduced cancer therapy at near infrared-II biowindow. *ACS Nano* **2018**, *12*, 4545–4555. [[CrossRef](#)]
21. Janczarek, M.; Endo-Kimura, M.; Wang, K.; Wei, Z.; Akanda, M.M.A.; Markowska-Szczupak, A.; Ohtani, B.; Kowalska, E. Is Black Titania a Promising Photocatalyst? *Catalysts* **2022**, *12*, 1320. [[CrossRef](#)]
22. Fu, Y.; Janczarek, M. Polyaniline–Titanium Dioxide Heterostructures as Efficient Photocatalysts: A Review. *Crystals* **2023**, *13*, 1637. [[CrossRef](#)]
23. Zhang, P.; Zhang, L.; Dong, E.; Zhang, X.; Zhang, W.; Wang, Q.; Xu, S.; Li, H. Synthesis of $\text{CaIn}_2\text{S}_4/\text{TiO}_2$ heterostructures for enhanced UV–visible light photocatalytic activity. *J. Alloys Compd.* **2021**, *885*, 161027. [[CrossRef](#)]
24. Kozak, M.; Mazierski, P.; Zebrowska, J.; Kobylanski, M.; Klimczuk, T.; Lisowski, W.; Trykowski, G.; Nowaczyk, G.; Zaleska-Medynska, A. Electrochemically Obtained $\text{TiO}_2/\text{Cu}_x\text{O}_y$ Nanotube Arrays Presenting a Photocatalytic Response in Processes of Pollutants Degradation and Bacteria Inactivation in Aqueous Phase. *Catalysts* **2018**, *8*, 237. [[CrossRef](#)]
25. Wang, K.; Bielan, Z.; Endo-Kimura, M.; Janczarek, M.; Zhang, D.; Kowalski, D.; Zielińska-Jurek, A.; Markowska-Szczupak, A.; Ohtani, B.; Kowalska, E. On the mechanism of photocatalytic reactions on $\text{Cu}_x\text{O}@/\text{TiO}_2$ core–shell photocatalysts. *J. Mat. Chem. A* **2021**, *9*, 10135–10145. [[CrossRef](#)]
26. Wei, Z.; Janczarek, M.; Endo, M.; Wang, K.L.; Balcytis, A.; Nitta, A.; Mendez-Medrano, M.G.; Colbeau-Justin, C.; Juodkazis, S.; Ohtani, B.; et al. Noble metal-modified faceted anatase titania photocatalysts: Octahedron versus decahedron. *Appl. Catal. B-Environ.* **2018**, *237*, 574–587. [[CrossRef](#)] [[PubMed](#)]

27. Wei, Z.; Kowalska, E.; Verrett, J.; Colbeau-Justin, C.; Remita, H.; Ohtani, B. Morphology-dependent photocatalytic activity of octahedral anatase particles prepared by ultrasonication-hydrothermal reaction of titanates. *Nanoscale* **2015**, *7*, 12392–12404. [[CrossRef](#)] [[PubMed](#)]
28. Wei, Z.S.; Kowalska, E.; Ohtani, B. Enhanced Photocatalytic Activity by Particle Morphology: Preparation, Characterization, and Photocatalytic Activities of Octahedral Anatase Titania Particles. *Chem. Lett.* **2014**, *43*, 346–348. [[CrossRef](#)]
29. Amano, F.; Yasumoto, T.; Mahaney, O.O.P.; Uchida, S.; Shibayama, T.; Terada, Y.; Ohtani, B. Highly Active Titania Photocatalyst Particles of Controlled Crystal Phase, Size, and Polyhedral Shapes. *Top. Catal.* **2010**, *53*, 455–461. [[CrossRef](#)]
30. Amano, F.; Prieto-Mahaney, O.O.; Terada, Y.; Yasumoto, T.; Shibayama, T.; Ohtani, B. Decahedral single-crystalline particles of anatase titanium(IV) oxide with high photocatalytic activity. *Chem. Mater.* **2009**, *21*, 2601–2603. [[CrossRef](#)]
31. Prieto-Mahaney, O.O.; Murakami, N.; Abe, R.; Ohtani, B. Correlation between photocatalytic activities and structural and physical properties of titanium(IV) oxide powders. *Chem. Lett.* **2009**, *38*, 238–239. [[CrossRef](#)]
32. Janczarek, M.; Kowalska, E.; Ohtani, B. Decahedral-shaped anatase titania photocatalyst particles: Synthesis in a newly developed coaxial-flow gas-phase reactor. *Chem. Eng. J.* **2016**, *289*, 502–512. [[CrossRef](#)]
33. Dozzi, M.V.; Selli, E. Specific Facets-Dominated Anatase TiO₂: Fluorine-Mediated Synthesis and Photoactivity. *Catalysts* **2013**, *3*, 455–485. [[CrossRef](#)]
34. Tachikawa, T.; Yamashita, S.; Majima, T. Evidence for Crystal-Face-Dependent TiO₂ Photocatalysis from Single-Molecule Imaging and Kinetic Analysis. *J. Am. Chem. Soc.* **2011**, *133*, 7197–7204. [[CrossRef](#)] [[PubMed](#)]
35. Ohtani, B.; Mahaney, O.O.P.; Amano, F.; Murakami, N.; Abe, R. What Are Titania Photocatalysts?—An Exploratory Correlation of Photocatalytic Activity with Structural and Physical Properties. *J. Adv. Oxid. Technol.* **2010**, *13*, 247–261. [[CrossRef](#)]
36. Ohtani, B. Photocatalysis A to Z—What we know and what we do not know in a scientific sense. *J. Photochem. Photobiol. C* **2010**, *11*, 157–178. [[CrossRef](#)]
37. Mino, L.; Pellegrino, F.; Rades, S.; Radnik, J.; Hodoroaba, V.-D.; Spoto, G.; Maurino, V.; Martra, G. Beyond Shape Engineering of TiO₂ Nanoparticles: Post-Synthesis Treatment Dependence of Surface Hydration, Hydroxylation, Lewis Acidity and Photocatalytic Activity of TiO₂ Anatase Nanoparticles with Dominant {001} or {101} Facets. *ACS Appl. Nano Mater.* **2018**, *1*, 5355–5365. [[CrossRef](#)]
38. Mino, L.; Zecchina, A.; Martra, G.; Rossi, A.M.; Spoto, G. A surface science approach to TiO₂ P25 photocatalysis: An in situ FTIR study of phenol photodegradation at controlled water coverages from sub-monolayer to multilayer. *Appl. Catal. B Environmen.* **2016**, *196*, 135–141. [[CrossRef](#)]
39. Wei, Z.; Wu, L.; Yue, X.; Mu, H.; Li, Z.; Chang, Y.; Janczarek, M.; Juodkakis, S.; Kowalska, E. Titania nanoengineering towards efficient plasmonic photocatalysis: Mono- and bi-metal-modified mesoporous microballs built of faceted anatase. *Appl. Catal. B Environ.* **2024**, *345*, 123654. [[CrossRef](#)]
40. Kowalski, D.; Mallet, J.; Thomas, S.; Rysz, J.; Bercu, B.; Michel, J.; Molinari, M. Self-organization of TiO₂ nanotubes in mono-, di- and tri-ethylene glycol electrolytes. *Electrochim. Acta* **2016**, *204*, 287–293. [[CrossRef](#)]
41. Kowalski, D.; Kim, D.; Schmuki, P. TiO₂ nanotubes, nanochannels and mesosponge: Self-organized formation and applications. *Nano Today* **2013**, *8*, 235–264. [[CrossRef](#)]
42. Wang, L.; Mogan, T.R.; Wang, K.; Takashima, M.; Ohtani, B.; Kowalska, E. Fabrication and Characterization of Inverse-Opal Titania Films for Enhancement of Photocatalytic Activity. *ChemEngineering* **2022**, *6*, 33. [[CrossRef](#)]
43. Raja-Mogan, T.; Lehoux, A.; Takashima, M.; Kowalska, E.; Ohtani, B. Slow photon-induced enhancement of photocatalytic activity of gold nanoparticle-incorporated titania in-verse opal. *Chem. Lett.* **2021**, *50*, 711–713. [[CrossRef](#)]
44. Bian, Z.F.; Tachikawa, T.; Zhang, P.; Fujitsuka, M.; Majima, T. Au/TiO₂ Superstructure-Based Plasmonic Photocatalysts Exhibiting Efficient Charge Separation and Unprecedented Activity. *J. Am. Chem. Soc.* **2014**, *136*, 458–465. [[CrossRef](#)]
45. Bian, Z.F.; Tachikawa, T.; Zhang, P.; Fujitsuka, M.; Majima, T. A nanocomposite superstructure of metal oxides with effective charge transfer interfaces. *Nat. Commun.* **2014**, *5*, 3038. [[CrossRef](#)] [[PubMed](#)]
46. Zhang, W.; He, H.L.; Tian, Y.; Lan, K.; Liu, Q.; Wang, C.Y.; Liu, Y.; Elzatahry, A.; Che, R.C.; Li, W.; et al. Synthesis of uniform ordered mesoporous TiO₂ microspheres with controllable phase junctions for efficient solar water splitting. *Chem. Sci.* **2019**, *10*, 1664–1670. [[CrossRef](#)] [[PubMed](#)]
47. Zhang, B.; Cao, S.; Du, M.; Ye, X.; Wang, Y.; Ye, J. Titanium Dioxide (TiO₂) Mesocrystals: Synthesis, Growth Mechanisms and Photocatalytic Properties. *Catalysts* **2019**, *9*, 91. [[CrossRef](#)]
48. Niederberger, M.; Cölfen, H. Oriented attachment and mesocrystals: Non-classical crystallization mechanisms based on nanoparticle assembly. *Phys. Chem. Chem. Phys.* **2006**, *8*, 3271–3287. [[CrossRef](#)] [[PubMed](#)]
49. Zhang, P.; Fujitsuka, M.; Majima, T. Development of tailored TiO₂ mesocrystals for solar driven photocatalysis. *J. Energy Chem.* **2016**, *25*, 917–926. [[CrossRef](#)]
50. Kraeutler, B.; Bard, A.J. Heterogeneous photocatalytic preparation of supported catalysts. Photodeposition of platinum on TiO₂ powder and other substrates. *J. Am. Chem. Soc.* **1978**, *100*, 4317–4318. [[CrossRef](#)]
51. Herrmann, J.-M.; Disdier, J.; Pichat, P. Photoassisted platinum deposition on TiO₂ powder using various platinum complexes. *J. Phys. Chem.* **1986**, *90*, 6028–6034. [[CrossRef](#)]
52. Ohtani, B.; Okugawa, Y.; Nishimoto, S.; Kagiya, T. Photocatalytic activity of titania powders suspended in aqueous silver nitrate solution: Correlation with pH-dependent surface structures. *J. Phys. Chem.* **1987**, *91*, 3550–3555. [[CrossRef](#)]
53. Nishimoto, S.I.; Ohtani, B.; Kagiya, T. Photocatalytic Dehydrogenation of Aliphatic-Alcohols by Aqueous Suspensions of Platinized Titanium-Dioxide. *J. Chem. Soc. Farad. Trans. 1 Phys. Chem. Condens. Phases* **1985**, *81*, 2467–2474. [[CrossRef](#)]

54. Sakai, N.; Fujiwara, Y.; Takahashi, Y.; Tatsuma, T. Plasmon-resonance-based generation of cathodic photocurrent at electrodeposited gold nanoparticles coated with TiO₂ films. *Chem. Phys. Chem.* **2009**, *10*, 766–769. [[CrossRef](#)] [[PubMed](#)]
55. Tian, Y.; Tatsuma, T. Mechanisms and Applications of Plasmon-Induced Charge Separation at TiO₂ Films Loaded with Gold Nanoparticles. *J. Am. Chem. Soc.* **2005**, *127*, 7632–7637. [[CrossRef](#)] [[PubMed](#)]
56. Bielan, Z.; Kowalska, E.; Dudziak, S.; Wang, K.; Ohtani, B.; Zielinska-Jurek, A. Mono- and bimetallic (Pt/Cu) titanium(IV) oxide core-shell photocatalysts with UV/Vis light activity and magnetic separability. *Catal. Today* **2021**, *361*, 198–209. [[CrossRef](#)]
57. Shi, J.; Chen, J.; Li, G.; An, T.; Yamashita, H. Fabrication of Au/TiO₂ nanowires@carbon fiber paper ternary composite for visible-light photocatalytic degradation of gaseous styrene. *Catal. Today* **2017**, *281*, 621–629. [[CrossRef](#)]
58. Kowalska, E.; Abe, R.; Ohtani, B. Visible light-induced photocatalytic reaction of gold-modified titanium(IV) oxide particles: Action spectrum analysis. *Chem. Commun.* **2009**, *2*, 241–243. [[CrossRef](#)] [[PubMed](#)]
59. Murugesan, S.; Kuppasami, P.; Parvathavarthini, N.; Mohandas, E. Pulsed laser deposition of anatase and rutile TiO₂ thin films. *Surf. Coat. Tech.* **2007**, *201*, 7713–7719. [[CrossRef](#)]
60. Pan, J.; Liu, G.; Lu, G.Q.; Cheng, H.-M. On the True Photoreactivity Order of {001}, {010}, and {101} Facets of Anatase TiO₂ Crystals. *Angew. Chem. Int. Ed.* **2011**, *50*, 2133–2137. [[CrossRef](#)]
61. Ye, J.; Liu, W.; Cai, J.; Chen, S.; Zhao, X.; Zhou, H.; Qi, L. Nanoporous Anatase TiO₂ Mesocrystals: Additive-Free Synthesis, Remarkable Crystalline-Phase Stability, and Improved Lithium Insertion Behavior. *J. Am. Chem. Soc.* **2011**, *133*, 933–940. [[CrossRef](#)]
62. Kelly, B.G.; Loether, A.B.; DiChiara, A.D.; Henning, R.W.; DeCamp, M.F.; Unruh, K.M. Lattice parameter evolution in Pt nanoparticles during photo-thermally induced sintering and grain growth. *J. Phys. Chem. Solids* **2017**, *108*, 104–108. [[CrossRef](#)]
63. Wei, Z.S.; Endo-Kimura, M.; Wang, K.L.; Colbeau-Justin, C.; Kowalska, E. Influence of semiconductor morphology on photocatalytic activity of plasmonic photocatalysts: Titanate nanowires and octahedral anatase nanoparticles. *Nanomaterials* **2019**, *9*, 1447. [[CrossRef](#)] [[PubMed](#)]
64. Wei, Z.; Endo, M.; Wang, K.; Charbit, E.; Markowska-Szczupak, A.; Ohtani, B.; Kowalska, E. Noble metal-modified octahedral anatase titania particles with enhanced activity for decomposition of chemical and microbiological pollutants. *Chem. Eng. J.* **2017**, *318*, 121–134. [[CrossRef](#)] [[PubMed](#)]
65. Yu, J.G.; Zhao, X.J.; Zhao, Q.N. Effect of surface structure on photocatalytic activity of TiO₂ thin films prepared by sol-gel method. *Thin Solid. Films* **2000**, *379*, 7–14. [[CrossRef](#)]
66. Reszczynska, J.; Grzyb, T.; Sobczak, J.W.; Lisowski, W.; Gazda, M.; Ohtani, B.; Zaleska, A. Visible light activity of rare earth metal doped (Er³⁺, Yb³⁺ or Er³⁺/Yb³⁺) titania photocatalysts. *Appl. Catal. B-Environ.* **2015**, *163*, 40–49. [[CrossRef](#)]
67. Reszczynska, J.; Grzyb, T.; Sobczak, J.W.; Lisowski, W.; Gazda, M.; Ohtani, B.; Zaleska, A. Lanthanide co-doped TiO₂: The effect of metal type and amount on surface properties and photocatalytic activity. *Appl. Surf. Sci.* **2014**, *307*, 333–345. [[CrossRef](#)]
68. Jensen, H.; Soloviev, A.; Li, Z.S.; Sogaard, E.G. XPS and FTIR investigation of the surface properties of different prepared titania nano-powders. *Appl. Surf. Sci.* **2005**, *246*, 239–249. [[CrossRef](#)]
69. Ono, L.K.; Yuan, B.; Heinrich, H.; Cuenya, B.R. Formation and Thermal Stability of Platinum Oxides on Size-Selected Platinum Nanoparticles: Support Effects. *J. Phys. Chem. C* **2010**, *114*, 22119–22133. [[CrossRef](#)]
70. Zheng, X.; Chan, M.H.-Y.; Chan, A.K.-W.; Cao, S.; Ng, M.; Sheong, F.K.; Li, C.; Goonetilleke, E.C.; Lam, W.W.Y.; Lau, T.-C.; et al. Elucidation of the key role of Pt··Pt interactions in the directional self-assembly of platinum(II) complexes. *Proc. Natl. Acad. Sci. USA* **2022**, *119*, e2116543119. [[CrossRef](#)]
71. Zhu, S.; Wang, X.; Luo, E.; Yang, L.; Chu, Y.; Gao, L.; Jin, Z.; Liu, C.; Ge, J.; Xing, W. Stabilized Pt Cluster-Based Catalysts Used as Low-Loading Cathode in Proton-Exchange Membrane Fuel Cells. *ACS Energy Lett.* **2020**, *5*, 3021–3028. [[CrossRef](#)]
72. Dvořák, F.; Farnesi Camellone, M.; Tovt, A.; Tran, N.-D.; Negreiros, F.R.; Vorokhta, M.; Skála, T.; Matolínová, I.; Mysliveček, J.; Matolín, V.; et al. Creating single-atom Pt-ceria catalysts by surface step decoration. *Nature Commun.* **2016**, *7*, 10801. [[CrossRef](#)] [[PubMed](#)]
73. Makuła, P.; Pacia, M.; Macyk, W. How To Correctly Determine the Band Gap Energy of Modified Semiconductor Photocatalysts Based on UV-Vis Spectra. *J. Phys. Chem. Lett.* **2018**, *9*, 6814–6817. [[CrossRef](#)]
74. Marić, I.; Dražić, G.; Ivanda, M.; Jurkin, T.; Štefanić, G.; Gotić, M. Impact of Fe(III) ions on the structural and optical properties of anatase-type solid solutions. *J. Mol. Struct.* **2019**, *1179*, 354–365. [[CrossRef](#)]
75. Nemashkalo, A.B.; Busko, T.O.; Peters, R.M.; Dmytrenko, O.P.; Kulish, M.P.; Vityuk, N.V.; Tkach, V.M.; Strzhemechny, Y.M. Electronic band structure studies of anatase TiO₂ thin films modified with Ag, Au, or ZrO₂ nanophases. *Phys. Status Solidi B Basic. Res.* **2016**, *253*, 1754–1764. [[CrossRef](#)]
76. Jain, P.K.; Huang, X.H.; El-Sayed, I.H.; El-Sayed, M.A. Noble metals on the nanoscale: Optical and photothermal properties and some applications in imaging, sensing, biology, and medicine. *Accounts Chem. Res.* **2008**, *41*, 1578–1586. [[CrossRef](#)]
77. Stietz, F.; Trager, F. Surface plasmons in nanoclusters: Elementary electronic excitations and their applications. *Philos. Mag.* **1999**, *79*, 1281–1298. [[CrossRef](#)]
78. Douketis, C.; Shalaev, V.M.; Haslett, T.L.; Wang, Z.; Moskovits, M. The role of localized surface plasmons in photoemission from silver films: Direct and indirect transition channels. *J. Electron. Spectrosc.* **1993**, *64/65*, 167–175. [[CrossRef](#)]
79. Xia, Y.N.; Xiong, Y.J.; Lim, B.; Skrabalak, S.E. Shape-Controlled Synthesis of Metal Nanocrystals: Simple Chemistry Meets Complex Physics? *Angew. Chem. Int. Edit.* **2009**, *48*, 60–103. [[CrossRef](#)]

80. Xia, Y.N.; Halas, N.J. Shape-controlled synthesis and surface plasmonic properties of metallic nanostructures. *MRS Bull.* **2005**, *30*, 338–344. [[CrossRef](#)]
81. Mock, J.J.; Barbic, M.; Smith, D.R.; Schultz, D.A.; Schultz, S. Shape effects in plasmon resonance of individual colloidal silver nanoparticles. *J. Chem. Phys.* **2002**, *116*, 6755–6759. [[CrossRef](#)]
82. Link, S.; El-Sayed, M.A. Spectral properties and relaxation dynamics of surface plasmon electronic oscillations in gold and silver nanodots and nanorods. *J. Phys. Chem. B* **1999**, *103*, 8410–8426. [[CrossRef](#)]
83. Kunwar, S.; Sui, M.; Pandey, P.; Gu, Z.; Pandit, S.; Lee, J. Improved Configuration and LSPR Response of Platinum Nanoparticles via Enhanced Solid State Dewetting of In-Pt Bilayers. *Sci. Rep.* **2019**, *9*, 1329. [[CrossRef](#)] [[PubMed](#)]
84. Wong, R.J.; Tsounis, C.; Scott, J.; Low, G.K.-C.; Amal, R. Promoting Catalytic Oxygen Activation by Localized Surface Plasmon Resonance: Effect of Visible Light Pre-treatment and Bimetallic Interactions. *Chemcatchem* **2018**, *10*, 287–295. [[CrossRef](#)]
85. Qin, Y.; Li, Y.; Tian, Z.; Wu, Y.; Cui, Y. Efficiently Visible-Light Driven Photoelectrocatalytic Oxidation of As(III) at Low Positive Biasing Using Pt/TiO₂ Nanotube Electrode. *Nanoscale Res. Lett.* **2016**, *11*, 32. [[CrossRef](#)] [[PubMed](#)]
86. Chelvayohan, M.; Mee, C.H.B. Work Function Measurements on (110), (100) and (111) Surfaces of Silver. *J. Phys. C Solid. State* **1982**, *15*, 2305–2312. [[CrossRef](#)]
87. Sachtler, W.M.H.; Dorgelo, G.J.H.; Holscher, A.A. The work function of gold. *Surf. Sci.* **1966**, *5*, 221–229. [[CrossRef](#)]
88. Sachtler, W.M.; Dorgelo, G.J.H. Surface of Copper-Nickel Alloy Films: I. Work Function and Phase Composition. *J. Catal.* **1965**, *4*, 654–664. [[CrossRef](#)]
89. Chen, Y.; Soler, L.; Cazorla, C.; Oliveras, J.; Bastús, N.G.; Puentes, V.F.; Llorca, J. Facet-engineered TiO₂ drives photocatalytic activity and stability of supported noble metal clusters during H₂ evolution. *Nat. Commun.* **2023**, *14*, 6165. [[CrossRef](#)] [[PubMed](#)]
90. Bumajdad, A.; Madkour, M. Understanding the superior photocatalytic activity of noble metals modified titania under UV and visible light irradiation. *Phys. Chem. Chem. Phys.* **2014**, *16*, 7146–7158. [[CrossRef](#)]
91. Ohtani, B.; Iwai, K.; Nishimoto, S.-i.; Sato, S. Role of Platinum Deposits on Titanium(IV) Oxide Particles: Structural and Kinetic Analyses of Photocatalytic Reaction in Aqueous Alcohol and Amino Acid Solutions. *J. Phys. Chem. B* **1997**, *101*, 3349–3359. [[CrossRef](#)]
92. Subramanian, V.; Wolf, E.; Kamat, P.V. Semiconductor-Metal Composite Nanostructures. To What Extent Do Metal Nanoparticles Improve the Photocatalytic Activity of TiO₂ Films? *J. Phys. Chem. B* **2001**, *105*, 11439–11446. [[CrossRef](#)]
93. Kisch, H. On the Problem of Comparing Rates or Apparent Quantum Yields in Heterogeneous Photocatalysis. *Angew. Chem. Int. Ed.* **2010**, *49*, 9588–9589. [[CrossRef](#)] [[PubMed](#)]
94. Minero, C.; Pellizzari, P.; Maurino, V.; Pelizzetti, E.; Vione, D. Enhancement of dye sonochemical degradation by some inorganic anions present in natural waters. *Appl. Catal. B-Environ.* **2008**, *77*, 308–316. [[CrossRef](#)]
95. Minero, C.; Maurino, V.; Pelizzetti, E.; Vione, D. An empirical, quantitative approach to predict the reactivity of some substituted aromatic compounds towards reactive radical species (Cl^{-2•}, Br^{-2•}, •NO₂, SO₃^{-•}, SO₄^{-•}) in aqueous solution. *Environ. Sci. Pollut. R.* **2006**, *13*, 212–214.
96. Buchalska, M.; Kobielski, M.; Matuszek, A.; Pacia, A.; Wojtyła, S.; Macyk, W. On Oxygen Activation at Rutile- and Anatase-TiO₂. *ACS Catal.* **2015**, *5*, 7424–7431. [[CrossRef](#)]
97. Liu, W.; Li, Y.; Liu, F.; Jiang, W.; Zhang, D.; Liang, J. Visible-light-driven photocatalytic degradation of diclofenac by carbon quantum dots modified porous g-C₃N₄: Mechanisms, degradation pathway and DFT calculation. *Water Res.* **2019**, *151*, 8–19. [[CrossRef](#)] [[PubMed](#)]
98. Chen, L.; Ji, H.; Qi, J.; Huang, T.; Wang, C.-C.; Liu, W. Degradation of acetaminophen by activated peroxydisulfate using Co(OH)₂ hollow microsphere supported titanate nanotubes: Insights into sulfate radical production pathway through CoOH⁺ activation. *Chem. Eng. J.* **2021**, *406*, 126877. [[CrossRef](#)]
99. Kowalska, E.; Rau, S.; Ohtani, B. Plasmonic Titania Photocatalysts Active under UV and Visible-Light Irradiation: Influence of Gold Amount, Size, and Shape. *J. Nanotechnol.* **2012**, *2012*, 361853. [[CrossRef](#)]
100. Herrmann, J.M.; Disdier, J.; Pichat, P.; Fernandez, A.; Gonzalez-Eliphe, A.; Munuera, G.; Leclercq, C. Titania-supported bimetallic catalyst synthesis by photocatalytic codeposition at ambient temperature: Preparation and characterization of platinum-rhodium, silver-rhodium, and platinum-palladium couples. *J. Catal.* **1991**, *132*, 490–497. [[CrossRef](#)]
101. Hussein, F.H.; Rudham, R. Photocatalytic dehydrogenation of liquid alcohols by platinumized anatase. *J. Chem. Soc. Faraday Trans. 1* **1987**, *83*, 1631–1639. [[CrossRef](#)]
102. Tanaka, K.; Harada, K.; Murata, S. Photocatalytic deposition of metal ions onto titanium dioxide powder. *Sol. Energy* **1986**, *36*, 159–161. [[CrossRef](#)]
103. Wei, Z.; Rosa, L.; Wang, K.; Endo, M.; Juodkazi, S.; Ohtani, B.; Kowalska, E. Size-controlled gold nanoparticles on octahedral anatase particles as efficient plasmonic photocatalyst. *Appl. Catal. B Environ.* **2017**, *206*, 393–405. [[CrossRef](#)] [[PubMed](#)]

Disclaimer/Publisher's Note: The statements, opinions and data contained in all publications are solely those of the individual author(s) and contributor(s) and not of MDPI and/or the editor(s). MDPI and/or the editor(s) disclaim responsibility for any injury to people or property resulting from any ideas, methods, instructions or products referred to in the content.